Temporal dependence of shifts in mu opioid receptor mobility at the cell surface after agonist binding observed by single-particle tracking

Marissa J. Metz,[1,*] Reagan L. Pennock,[1,*] Diego Krapf,[2,3,†] and Shane T. Hentges[1,†]

[1] *Department of Biomedical Sciences, Colorado State University, Fort Collins, CO, USA*
[2] *Department of Electrical and Computer Engineering, Colorado State University, Fort Collins, CO, USA*
[3] *School of Biomedical Engineering, Colorado State University, Fort Collins, CO, USA*

There is a need to identify mu opioid receptor (MOR) agonists that can preferentially activate certain signaling pathways over others in order to develop better analgesics with reduced side effects. The present study aimed to determine if single-particle tracking (SPT) of the MOR could provide a robust sensor for distinct signaling states without reliance on effector-based readouts. SPT of quantum dot labeled FLAG-tagged MORs in AtT20 cells was performed. Under basal conditions, mobile and immobile states of FLAG-MORs were found to coexist on the plasma membrane. After cells were treated acutely with the MOR agonist DAMGO, there was a higher fraction of mobile trajectories and free portions of the mobile tracks resulted, in part, from G-protein interaction. After 10 minutes of agonist exposure, the population of immobile receptors increased, as did co-localization with clathrin. Yet, no single mobility state could fully account for colocalization with clathrin. Prior discrepant reports of MOR mobility may be attributable to the limitations of population assessments and use of a single exposure duration, which the current approach overcomes. Despite the advantages, it appears that the SPT approach will be most informative when effectors are examined simultaneously with the receptors.

INTRODUCTION

The mu opioid receptor (MOR) is a G-protein coupled receptor (GPCR) responsible for the analgesic effects of exogenously administered opioids (e.g. morphine, codeine, fentanyl). Signaling through the MOR also conveys negative side effects, potentially through specific signaling pathways. Thus, there is interest in identifying agonists that may preferentially activate select intracellular signaling pathways, such that analgesic actions are maintained while unwanted actions are minimized. The intracellular alterations induced by agonist binding to the MOR includes inhibition of adenylyl cyclase, inhibition of voltage-dependent Ca^{2+}-channels, activation of G-protein coupled inwardly rectifying K^+ channels, activation of signaling cascades that alter transcription, receptor phosphorylation, and receptor interaction with β-arrestin and clathrin-coated pits (CCPs), and these can vary by cell type and subcellular localization of the receptor [1, 2]. Most functional studies of the MOR have focused on the output produced by the inhibition or activation of effectors, as this generally provides a good proxy for signaling through the receptor. Often, however, such effector-based assays report the mean response across the population of receptors and can have limited spatial and temporal resolution. Further, readouts for each effector of interest can have distinct sensitivity and resolution, and assays for each effector are usually performed separately from one another. This makes it difficult to determine the relative engagement of select effectors in response to an agonist.

Imaging-based studies of directly labeled MORs have provided an alternative to effector-dependent assays and have been used to examine MOR mobility [3–9] and subcellular localization [5, 10–12]. Studies of MOR mobility utilizing fluorescence recovery after photobleaching (FRAP) and fluorescence correlation spectroscopy (FCS) have shown that MORs can exist in a variety of mobility states on the membrane. However, existing studies suggest that agonist binding either increases [6, 9] or decreases [7] lateral mobility of MORs. These conflicting results may be due to the use of different cell lines, different experimental conditions (e.g. temperature and agonist exposure duration) and the fact that these experiments relied on bulk approaches that reflect average mobility of the receptors as a population.

Single-particle tracking (SPT) approaches allow for examination of individual receptor behavior without reliance on effector-based readouts. Specific mobility states of individual receptors detected with SPT may correlate with distinct interactions with select effectors and other binding partners. Prior studies examining MOR mobility using SPT have shown differing results as to what these distinct mobility states are. One study tracking the MOR reported that most receptors are confined within mobile microdomains, while a smaller fraction of receptors exhibit slow, directed diffusion [4]. Another study reported short-term confinement and significant diffusion of the receptor between compartments on the cell membrane [8]. Importantly, neither of these studies examined the effect of agonist binding on MOR mobility, nor did they attribute specific mobility states to specific effector interactions.

The present study was designed to determine if SPT

* These authors contributed equally to this work
† These authors contributed equally to this work (email: diego.krapf@colostate.edu; shane.hentges@colostate.edu)

could provide a reliable approach to detect agonist-induced changes in mobility that correspond to interactions with G-proteins and recruitment to CCPs. Tracking of the MOR was performed in AtT20 cells stably expressing a FLAG-epitope-tagged MOR construct (FLAG-MOR) [13] conjugated with quantum dots (Qdots) conjugated via an anti-FLAG antibody. Signaling through MORs has been extensively characterized in AtT20 cells [13–15]. MORs in AtT20 cells couple to endogenously-expressed GIRKs [14, 16], P/Q-type VDCCs [13], adenylyl cyclase [17], and G-protein coupled receptor kinases [14, 18] via pertussis-toxin sensitive $G\alpha_{textrmi/o}$ proteins [19]. Further, AtT20 cells stably expressing FLAG-MORs exhibit relatively consistent and moderate expression of the receptor with activation, desensitization, and internalization phases similar to MORs in neurons [13]. Thus, AtT20 cells stably transfected with Flag-MOR provides a good system for examining real-time dynamics of the MOR in the plasma membrane before and during agonist exposure.

Here, MOR mobility was investigated before drug, after 1 min of exposure to the MOR agonist DAMGO (when some desensitization has occurred but internalization has not fully commenced), and after 10 min of DAMGO treatment (when desensitization is complete and internalization is occurring) [13]. Quantitative diffusion analysis of trajectories of Qdot 565-conjugated FLAG-MORs shows that receptors can be found in both relatively immobile and mobile states under basal conditions. Activation of FLAG-MORs with the full MOR agonist DAMGO results in an initial increase in the population of mobile receptors (after 1 min agonist exposure) followed at later time points (10 min agonist exposure) by a decrease in the mobile fraction. The findings show that activation of the FLAG-MOR does not result in a uniform decrease in the mobility of the receptors, but instead dynamically changes the fraction of FLAG-MORs found in more mobile or immobile states depending upon time observed after agonist exposure. Further, investigation of receptors in the mobile state revealed transient confinement influenced by G-protein binding. However, inspection of tracks later after agonist exposure revealed that mobility state was a poor proxy for colocalization with CCPs. The results indicate that ensemble measurements of receptor mobility, such as average mean square displacement (MSD), may not capture the full extent of receptor activity, and that single-particle tracking can better account for heterogeneity in signaling states. Altogether, mobility state can provide some information about signaling state, but may not account for the range of potential effectors a receptor is coupled to.

RESULTS

In order to visualize MORs, FLAG-MORs in AtT20 cells were labeled with Qdots. Cells were imaged under differential interference contrast to assess cell morphology

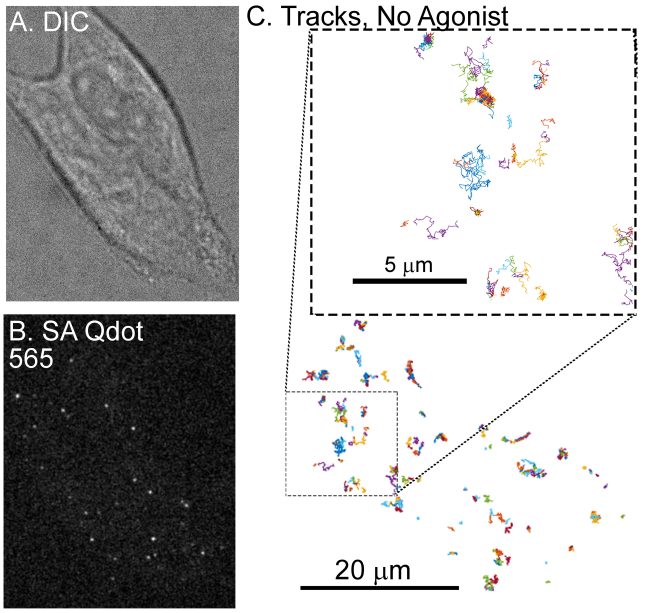

FIG. 1. Single-particle tracking of FLAG-MORs in AtT20 cells. A) A DIC image of an AtT20 cell and (B) a fluorescent image of SA Qdot 565 conjugated FLAG-MORs in the same cell. Labeling density in this image is typical for experiments carried out in this study. C) Trajectories of SA Qdot 565-conjugated FLAG-MORs imaged in the absence of drug from the cell shown in (A) and (B). All of the trajectories obtained from a single 1000 frame video segment are shown. The upper square in (C) shows an enlarged image of trajectories from the area indicated by the lower dashed box. Both mobile and immobile trajectories can be seen in the inset, as well as confined and free portions of mobile trajectories.

(Fig. 1A) and under fluorescence using spinning disk confocal to detect Qdots (Fig. 1B). Trajectories of labeled FLAG-MOR were obtained (Fig. 1C). FLAG-MOR mobility was investigated before agonist application, after 1 min of treatment with the agonist DAMGO, and after 10 min of exposure to DAMGO. Displacements of individual Qdot-MORs at increasing lag times were calculated from 50 ms to 2.5 s to obtain MSDs for each experimental condition. Time averaged MSD $\overline{\delta^2(t_{lag})}$ of individual Qdot-MOR trajectories were computed for time lags t_{lag} up to 2.5 s for each experimental condition (Eq. 1 in Materials and Methods). Fig. S1 shows a representative set of individual MSDs for trajectories in the no drug condition. Most trajectories appear to exhibit subdiffusive behavior, i.e., the MSD of individual trajectories is not linear in lag time but it scales as a power law $\overline{\delta^2(t_{lag})} = K_\alpha t_{lag}^\alpha$ with $\alpha < 1$, where α is the anomalous exponent and K_α is the generalized diffusion coefficient [20–22]. Furthermore, a substantial number of trajectories have a flat MSD, indicating that these particles are either immobile or confined to small domains [23]. In all cases, only particles that were observed for at least 3 s were analyzed. Clear differences were observed between the MSD under basal conditions and those in cells treated

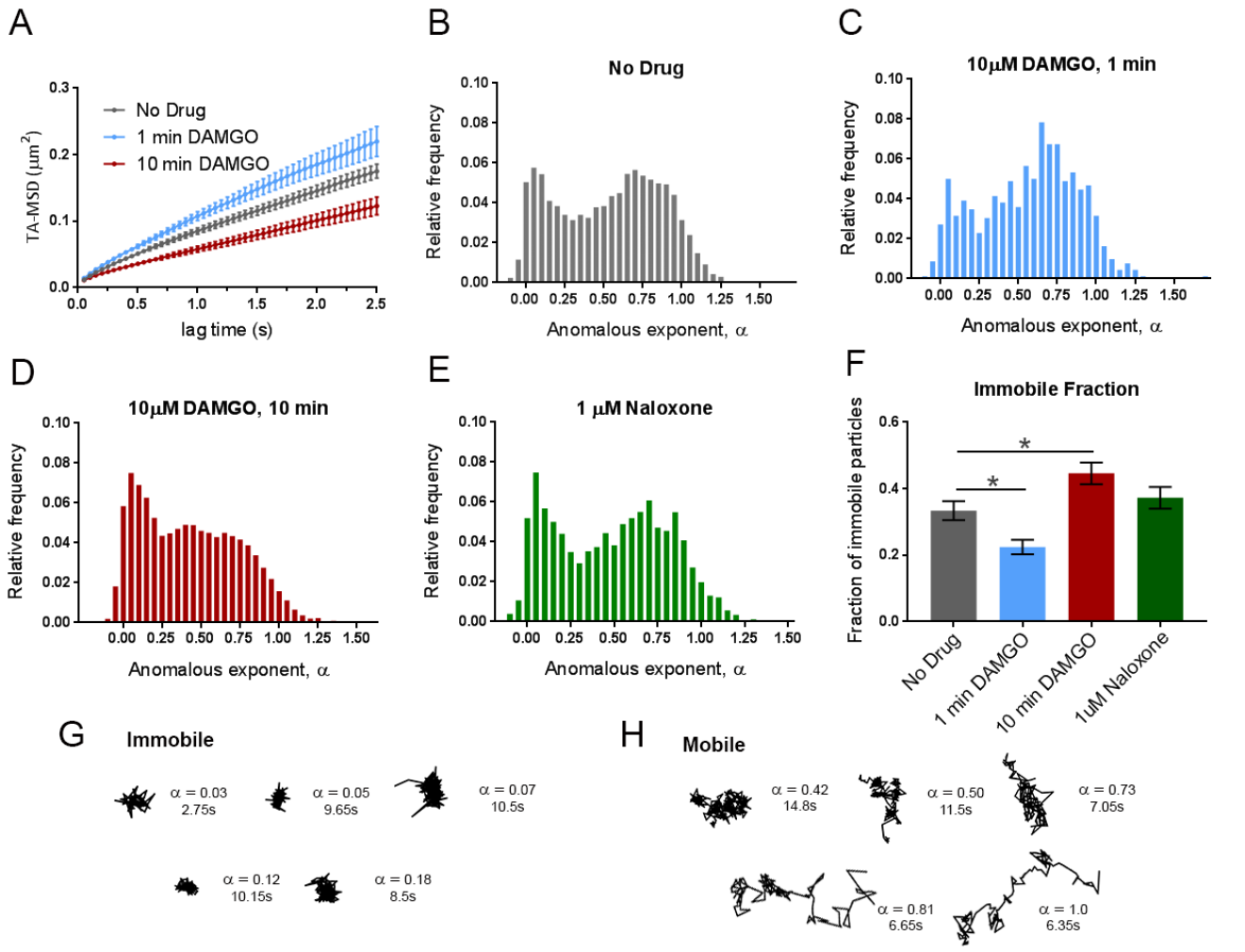

FIG. 2. Dynamic changes in MOR mobility exist depending upon the time of drug application. A) Time averaged MSD for all tracks for each experimental condition showing increases in the MSD with 1 min DAMGO treatment and decreases with 10 min DAMGO treatment. Distribution of anomalous exponents , obtained from the TA-MSD of individual trajectories for all tracks in the B) no drug ($n = 17$ cells, 8465 trajectories), C) 1 min DAMGO ($n = 12$ cells, 930 trajectories), D) 10 min DAMGO ($n = 13$ cells, 8465 trajectories), E) and Naloxone ($n = 7$ cells, 8227 trajectories) condition. All conditions exhibit bimodal distributions with peaks centered at $\alpha = 0.09$ and $\alpha = 0.71$for immobile and mobile populations, respectively. F) Compared to the no drug condition, the population of $\alpha = 0.27$ decreases in the 1 min DAMGO condition, increases in the 10 min DAMGO condition, and does not change after Naloxone application. Example trajectories from G) immobile ($\alpha < 0.27$) and H) mobile ($\alpha > 0.27$) populations are shown with their corresponding values and lengths. *$p < 0.05$, Kruskall-Wallis one-way ANOVA with multiple comparisons using Bonferroni correction, error bars represent SEM for cells.

with DAMGO (Fig. 2A). Short DAMGO treatment (1 min) increased the anomalous exponent α of the average MSD from 0.49 ± 0.12 in the no drug condition to 0.55 ± 0.02. In contrast, longer DAMGO treatment (10 min) decreased the anomalous exponent of the average MSD to 0.38 ± 0.02 ($p = 0.014$). Further, the generalized diffusion coefficient, K_α, of the averaged MSD increased after the 1 min DAMGO exposure from 0.087 ± 0.005 $\mu m^2/s^{0.49}$ (no drug condition) to 0.104 ± 0.006 $\mu m^2/s^{0.55}$ ($p = 0.034$), whereas longer DAMGO exposure (10 min) decreased the generalized diffusion coefficient to 0.057 ± 0.004 $\mu m^2/s^{0.38}$ ($p = 0.0004$ compared to no drug).

Ensemble measurements, such as average MSD, may mask important characteristics in the data that can be unmasked by looking at individual trajectories. Thus, the anomalous exponent was computed for individual trajectories in each experimental condition. Very low anomalous exponents are indicative of particles that explore a small region and present a flat MSD while larger exponents indicate that the trajectory explores a larger region and the MSD increases with lag time [24]. The histogram for the no-drug condition shows a large scat-

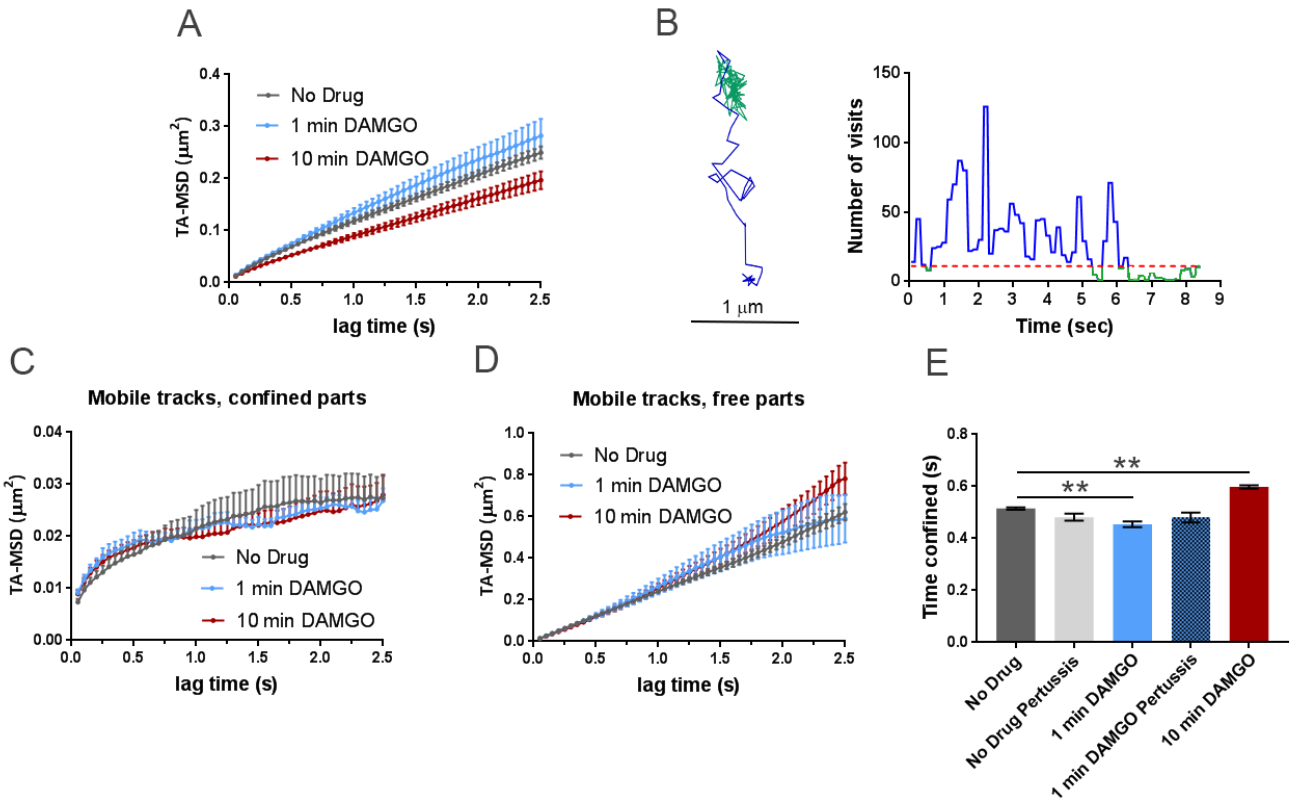

FIG. 3. Differences between MSD of mobile tracks can be explained by differences in dwell times between experimental conditions and G-protein binding. A) MSDs of mobile trajectories decreased after DAMGO treatment (10 min, $p = 0.031$). No drug (n=5855 trajectories), 1 min DAMGO (n= 697 trajectories), 10 min DAMGO (n=3958 trajectories). B) Example of a mobile track separated into free (blue) and confined (green) parts based on procedure described in Materials and Methods and published by Sikora et. al [30]. A threshold of 11 visits inside the circle was used to define confined portions (red dotted line). The right panel shows a time series of the number of visitations inside the circle for the example track shown, and free and confined portions are colored as in the example track. When segmented into C) confined and D) free portions, the MSDs are no longer different (confined $p = 0.150$, free $p > 0.99$). E) Confined dwell times decrease after acute DAMGO treatment and increase with longer DAMGO treatment. Application of 100 ng PTX prevents the decrease in confined dwell times seen after 1 min of DAMGO treatment. $^{**}p < 0.01$, Kruskall-Wallis one-way ANOVA with multiple comparisons using Bonferroni correction, error bars represent SEM for individual tracks.

tering of values, indicating marked heterogeneity in the diffusion behavior of FLAG-MORs (Fig. 2B). In particular, two populations are clearly visible, one with a narrow distribution centered at $\alpha = 0.09$ and another with a broader distribution centered at $\alpha = 0.71$. These populations can be separated at $\alpha \approx 0.27$, and examination of tracks within these two populations shows more confinement in the low population, and less confinement in the high population (Fig. 2G, H). Henceforth, tracks with $\alpha < 0.27$ are referred to as immobile and tracks with $\alpha \geq 0.27$ are referred to as mobile. After 1 min of DAMGO exposure, these two populations are still present, although a higher fraction of trajectories are in the mobile population (Fig. 2C). This trend is reversed in cells exposed to DAMGO for 10 min, where there is an increase in the fraction of immobile trajectories (Fig. 2D). To determine if ligand binding, rather than receptor activation was affecting mobility, cells were treated with the neutral antagonist Naloxone, which binds the receptor but does not induce signaling. Naloxone did not change the fraction of receptors in the immobile state (Fig. 2E), indicating that ligand binding alone was not sufficient to cause a mobility shift. The fraction of immobile tracks in each condition is shown in Fig. 2F. In the no drug condition, the immobile fraction is 0.33 ± 0.03 and it decreases to 0.23 ± 0.02 in the 1 min DAMGO condition ($p = 0.024$). Conversely, 10 min of DAMGO exposure resulted in an increase in the fraction of immobile trajectories to 0.45 ± 0.03. As expected, there is no significant change in the fraction of immobile trajectories caused by the neutral antagonist Naloxone (0.37 ± 0.03, $p = 0.147$ compared to the no drug condition).

Despite the advantages of Qdot labeling in terms of brightness and photostability [25–27], quantum dots have

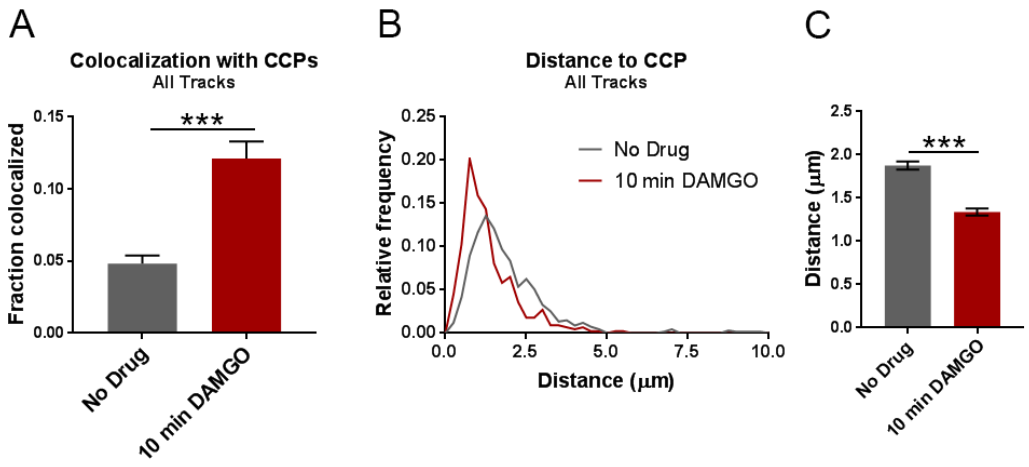

FIG. 4. Colocalization with CCPs increases across all tracks after DAMGO (10 min) application. A) When comparing all tracks, colocalization with CCPs increases after 10 min of DAMGO treatment. No drug $n = 9$ cells, 670 trajectories; 10 min DAMGO $n = 8$ cells, 446 trajectories. B) Distribution of distances to CCPs is shifted lower after 10 min of DAMGO treatment; combined data is represented in the bar graph. C) Combined data from (B) showing an overall decrease in the distance to CCPs for MORs treated with DAMGO for 10 min. ***$p < 0.0001$, Kruskall-Wallis one-way ANOVA with multiple comparisons using Bonferroni correction, error bars represent SEM for individual tracks.

the potential to reduce surface protein mobility [28]. Further, antibody-based detection has the potential to cause receptor crosslinking. To address these potential concerns, we compared our results with Qdot-labeled MORs to measurements of Flag-MOR bound to the fluorescent agonist Dermorphin-488 [29]. Exposure to Dermorphin-488 (10 min) results in α values similar to those obtained after 10 min of DAMGO exposure in cells with Qdot-labled MORs (Fig. S2). Thus, we exclude Qdot artifacts and crosslinking as the root for the immobilization observed. Overall, the findings indicate that the MOR shows dynamic alterations in mobility depending upon whether it is observed 1 or 10 min after drug treatment.

Next, we focused on the behavior of mobile tracks since we found that within mobile tracks prolonged DAMGO treatment (10 min) lowers MSDs compared to no drug or 1 min exposure. The anomalous exponent of the average MSD for mobile trajectories in the no drug condition was 0.62 ± 0.01. After 1 min of DAMGO exposure it was 0.65 ± 0.02, and after 10 min of DAMGO exposure it was 0.54 ± 0.03. Further, the K_α of the averaged MSD for mobile trajectories was 0.11 ± 0.02 $\mu m^2/s^{0.62}$ in the no drug condition and 0.12 ± 0.03 $\mu m^2/s^{0.65}$ in the 1 min DAMGO condition, whereas it was 0.087 ± 0.019 $\mu m^2/s^{0.54}$ in the 10 min DAMGO condition ($p = 0.041$, no drug compared to 10 min DAMGO). This result suggests that even within the mobile population of receptors, prolonged agonist exposure may lead to relatively reduced mobility. To examine this more closely we used a recently published method based on recurrence statistics [30] to further segment mobile trajectories ($\alpha > 0.27$) into confined and free portions. Briefly, for each two consecutive locations in a trajectory, a circle is drawn with its center halfway between them and the number of visits within this circle is counted. Periods that undergo confinement revisit the same region many times and thus the recurrence statistic is very high [30]. However, during free periods, particle exploration is less compact and thus the recurrence statistic is low (Fig 3B).

After segmenting the mobile trajectories into free and confined states, the MSDs of free and confined states do not differ between experimental conditions (confined $p = 0.150$, free $p > 0.99$, Figs. 3C & D). To better understand this narrowing in the MSD values between experimental conditions after recurrence analysis segmentation, we measure the dwell times of trajectories within free and confined states. One minute of DAMGO treatment decreased the time mobile tracks spend confined from 0.515 ± 0.004 s to 0.454 ± 0.011 s ($p < 0.0001$) and 10 min DAMGO increases confined periods to 0.598 ± 0.006 s ($p < 0.0001$, Fig 3E).

We next investigated which particular signaling interactions the free and confined portions of mobile trajectories represent by treating cells with pertussis toxin (PTX, 100 ng) overnight to inhibit G-protein/receptor interactions and again examined dwell times in free and confined portions of mobile tracks. Treatment with PTX without subsequent application of drug does not change confined dwell times of mobile trajectories (0.482 ± 0.014 s, $p = 0.45$, $n = 9$ cells; Fig. 3E, second bar). PTX treatment eliminates the increase free time for mobile tracks otherwise seen after applying DAMGO for 1 min (0.481 ± 0.019 s, $p > 0.99$ compared to no drug, $n = 14$ cells, Fig 3E, fourth bar). Therefore, G-protein binding appears to contribute to the time mobile trajectories spend in the free state.

Previous work indicates that after 10 min of DAMGO treatment, half of Flag-MORs in AtT20 cells have been

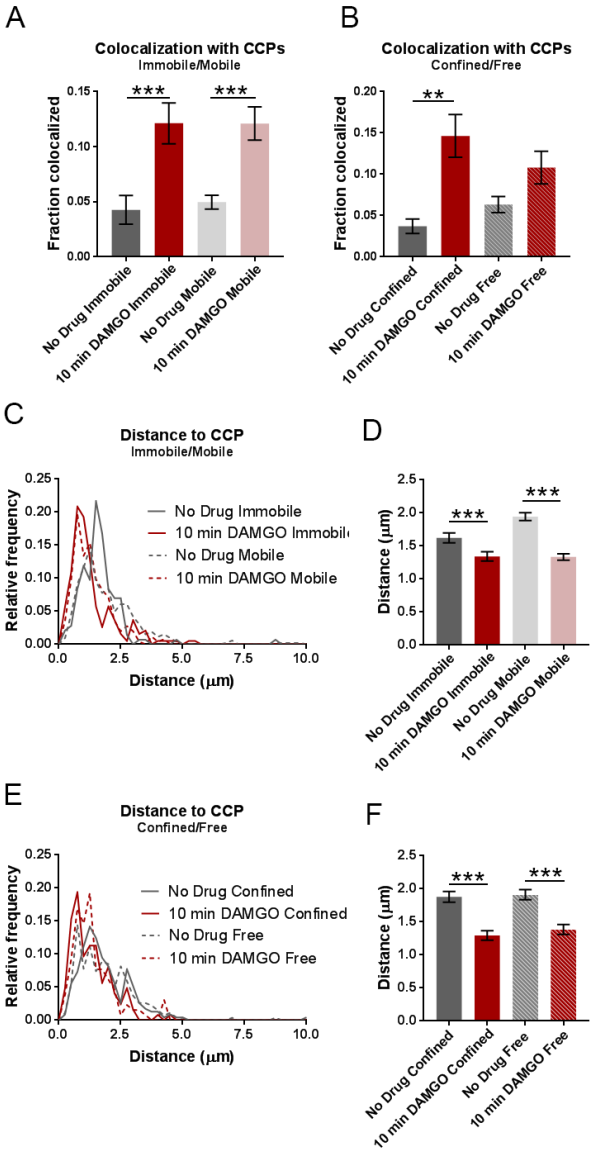

FIG. 5. Mobility state does not reflect colocalization with clathrin. A) Colocalization with CCPs does not differ between immobile and mobile populations within either the no drug nor the 10 min DAMGO experimental conditions. However, 10 min DAMGO still increases the fraction of MORs colocalized with CCPs both in mobile and immobile populations compared to no drug. B) Colocalization with CCPs also does not differ between confined and free portions of mobile tracks within the 10 min DAMGO or no drug experimental conditions. C) Distance to CCPs is decreased between no drug and 10 min DAMGO experimental conditions, but is not different between immobile and mobile fractions within experimental conditions. D) Combined data from (C) shows a clear lack of difference for distance to CCPs between immobile and mobile fractions from no drug and DAMGO treated cells. E) Distance to CCPs is not changed between confined and free portions of mobile tracks within either no drug or 10 min DAMGO conditions. F) Combined data from (E). $^{**}p < 0.01$, $^{***}p < 0.0001$, Kruskall-Wallis one-way ANOVA with multiple comparisons using Bonferroni correction, error bars represent SEM for individual tracks.

internalized and internalization is over half maximal [13]. Because of the observed shift towards lower values after 10 min of DAMGO treatment in our study, we hypothesized that capture into CCPs accounted for this shift towards receptor immobility. Thus we examined colocalization of the MOR with GFP-labeled clathrin light chain (GFP-CLC) [27, 31–33] puncta. Ten minutes of DAMGO treatment increased colocalization with GFP-CLC (from $4.8 \pm 0.6\%$ to $12.1 \pm 1.2\%$, $p < 0.0001$, Fig. 4A), and the distance to GFP-CLC was reduced by drug treatment (from 1.88 ± 0.05 m to 1.34 ± 0.04 m, $p < 0.0001$, Figs. 4B & C). However, the immobile population of receptors was not more colocalized with GFP-CLC than the mobile population of receptors in the 10 min DAMGO condition (immobile $12.1 \pm 1.9\%$ vs mobile $12.1 \pm 1.5\%$, p = 0.54, Fig. 5A). Distance to GFP-CLC was also unchanged between mobile and immobile populations after 10 min of DAMGO treatment (immobile 1.34 ± 0.07 μm vs mobile 1.33 ± 0.05 μm, $p = 0.18$, Figs. 5C & D). Inspection of GFP-CLC colocalization within the confined and free portions of mobile receptors after 10 min of DAMGO treatment showed that neither of these populations fully accounted for GFP-CLC colocalization (confined $14.6 \pm 2.6\%$ vs free $10.8 \pm 2.0\%$, $p = 0.99$, Fig. 5B). Distance to GFP-CLC was also unchanged between free and confined portions of mobile tracks (confined 1.29 ± 0.07 μm vs free 1.38 ± 0.07 μm, $p = 0.32$, Fig. 5E, F). Thus, mobility itself is not a good proxy for association with CCPs.

DISCUSSION

The present single-molecule study was undertaken to characterize time-dependent changes in FLAG-MOR diffusion induced by acute and extended applications of the full MOR agonist DAMGO and to understand if specific mobility states of the MOR could clearly reflect interactions with specific effectors. Under basal conditions, both mobile and immobile populations of FLAG-MORs were detected, evident in the bimodal distribution of the anomalous exponent . This bimodal distribution was skewed towards more mobile tracks for FLAG-MORs on cells that were exposed to a maximal concentration of DAMGO (10 μM) for one minute. However, DAMGO treatment for ten minutes resulted in a dramatic increase in the proportion of immobile FLAG-MORs. Closer inspection of mobile ($\alpha > 0.27$) tracks revealed that differences in MSD exist between experimental conditions even within the mobile subpopulation of receptors, and that this difference in MSD can be explained by an increase in confined dwell times of receptors treated with DAMGO for ten minutes. In contrast, MORs treated with DAMGO for one minute show a decrease in confined dwell times, and blockade of G-protein binding with pertussis toxin abrogates this decrease in confined period dwell times. Finally, CCP colocalization occurred similarly across all mobility states inspected so that a single

mobility state could not fully account for colocalization of FLAG-MORs with CCPs.

Previous studies of MOR mobility in response to agonist treatment have examined mobility at a minimum of ten minutes post-drug, although acute signaling processes occur much faster than this. In AtT20 cells, the receptor has already undergone G-protein coupling, desensitization, and internalization at this time point [13]. Thus, we were interested in understanding how MOR mobility is changed before internalization has begun and while the process of signaling and desensitization are occurring. The marked difference in receptor mobility depending upon duration of agonist exposure reveals that mobility is likely dependent on receptor interactions with intracellular partners. To our knowledge, the only other study investigating the mobility of the MOR in response to DAMGO at physiological temperature and at a similar time to ours found that lateral mobility of the MOR increases after DAMGO (1 μM) exposure for ten minutes [6]. This finding is in opposition to our observations at ten minutes post-DAMGO. This difference could be caused by differences in expression of, or interaction with, signaling partners between HEK293 cells and AtT20 resulting in distinct time course of MOR signaling. For example, Halls et al. discovered that it takes at least 60 minutes to see an increase in colocalization with CCPs in HEK293 cells5. Although we were not able to attribute receptor immobility to CCP colocalization, we did observe an increase in colocalization after ten minutes in the presence of DAMGO in AtT20 cells. It is also possible that other processes causing immobilization of the MOR are slowed in HEK cells compared to AtT20s.

Other processes besides capture into CCPs could account for the decrease in receptor mobility after ten minutes of DAMGO treatment. For example, protein kinase C has been found to restrict the distribution of the MOR in cell membranes [5], and it is possible that other kinases could contribute to immobility as well. Another study demonstrated colocalization of MORs with caveolin-1, which is a marker of putative lipid rafts [34]. Another study by the same group found that translocation into and out of these domains was agonist dependent, and that receptors located within the rafts were responsible for G-protein dependent signaling, while receptors located outside of the rafts were responsible for β-arrestin dependent signaling [35]. It is possible that these raft domains could contribute to the immobile receptor population observed after ten minutes of DAMGO treatment. However, it is worth noting that two other studies did not find MORs localized in the Triton X-100 insoluble membrane fractions thought to contain lipid rafts either before or after treatment with the agonist [5, 7]. Based on our finding that colocalization with CCPs cannot fully account for any single mobility state, it is likely that this is also true for other effectors as well. The immobile fraction of receptors after ten minute DAMGO treatment is likely due to the contribution of several effectors.

It was initially surprising to note that acute DAMGO treatment resulted in a decrease in the time that mobile tracks spent confined. However, a recent study by revealed that G-protein coupled receptors and their respective G-proteins couple at specific hot spots at least partially defined by actin networks [36]. Because desensitization is known to occur very quickly in AtT20 cells, perhaps the decrease in confined dwell times reflects the uncoupling of the receptor from G-proteins at hot spots. Alternatively, perhaps signaling receptors in AtT20 cells quickly hop between G-protein hot spots after activation of G-proteins, thus decreasing their confined dwell times. This possibility is supported by the fact that PTX restored confinement periods back to baseline levels, potentially suggesting that ligand-bound receptors are recruited to hot spots but cannot leave unless they have encountered a G-protein. Future studies using receptors that do not desensitize, such as non-phosphorylatable mutants [16, 37], could best parse apart the contribution of desensitization and G-protein coupling to transient confinement in mobile MOR trajectories.

Because CCP colocalization was not associated with a particular mobility population that we identified, it is unlikely that single-particle tracking of the MOR alone would be a good proxy for distinct receptor signaling states. However, concurrent tracking of the MOR with its signaling effectors may still be useful as a tool for biased agonist screening and for studies of receptor/effector interaction. For example, concurrent single-particle tracking of the MOR, G-proteins, and β-arrestin or CCPs would allow for screening of ligand bias within the same cell with high temporal resolution and individual receptor sensitivity. Ultimately, future studies using concurrent tracking of the MOR and effectors in neurons stands to provide new insight into receptor regulation and function while avoiding technical issues encountered with bulk assays, cell-lines, and single-time point observations.

MATERIALS AND METHODS

Cell Culture and Transfection

AtT20 cells stably expressing the FLAG-MOR (provided by Dr. MacDonald Christie, University of Sydney) were maintained at 37C/5% CO_2 in Dulbeccos Modified Eagle Medium (DMEM) supplemented with 10% fetal bovine serum (ATCC), L-Glutamine (2 mM L-alanyl-L-glutamine), and 1% penicillin/streptomycin. Once cells reached confluence they were exposed to 0.25% trypsin-EDTA (Gibco) and re-plated at lower density. Cells were maintained for no more than 12 passages beyond their original plating.

N-terminally tagged GFP-clathrin light chain (GFP-CLC, provided by Dr. Michael Tamkun, Colorado State University) was transfected into cells using 1:500 Lipofectamine (Invitrogen), 1:100 Opti-MEM (Gibco), and 1:1000 plasmid into 2 mL of culture media. Cells were incubated overnight, and all cells were imaged within 24

hours of transfection in order to avoid problems with overexpression. For experiments in which G-protein activity was inhibited, cells were treated with 100 ng pertussis toxin (Thermo Fisher) overnight. Cells were imaged within 24 hours of toxin treatment.

Live-Cell Labeling of the MOR

To prepare for imaging, AtT20 cells were diluted and plated on glass-bottom dishes (MatTek, Ashland, MA) containing the same supplemented DMEM solution as described above. Cells were imaged on the fourth day after plating. Labeling was performed immediately before imaging. Cells were rinsed multiple times with a saline solution containing: 35 mM KCl, 120 mM NaCl, 1 mM $CaCl_2$, 25 mM HEPES, 10 mM glucose, and pH was adjusted to 7.4 (NaOH). After thoroughly washing to remove DMEM, the plates were filled with saline containing 1% (w/v) bovine serum albumin (BSA, Sigma A7030) and incubated for 10 min at 37°C. The cells were incubated for 5 min at 37°C in the presence of a biotinylated anti-FLAG antibody (final concentration 1 μg/mL, BioM2 Anti-FLAG, Sigma F9291). After multiple rinses with saline (still containing 1% BSA) to remove unbound antibody, the cells were then incubated for 8 min at 37°C in the presence of streptavidin-coated quantum dots (1:10000, final concentration of 100 pM, Streptavidin Qdot 565, Life Technologies Q10133MP; or for two-color TIRF imaging Streptavidin Qdot 655, Life Technologies Q10121MP). The cells were rinsed multiple times with saline lacking BSA to remove unbound SA Qdot and BSA from the culture dish. In the 10 min DAMGO condition and Naloxone condition, 10 μM DAMGO or 1 μM Naloxone, respectively, was applied immediately after labeling. Drug was applied 10 min after the final wash on the microscope stage in the 1 min (10 μM) DAMGO condition. Many cells did not exhibit Qdot fluorescence upon imaging, so only those that had a moderate amount of labeling were chosen for imaging.

Confocal Microscopy

Single-channel imaging was carried on a spinning disk confocal microscope (Olympus IX83, Olympus UPlanSApo 100x/1.40 oil objective, Yokogawa CSU-X spinning disk, Andor iXon Ultra 897 EMCCD camera) equipped with a temperature control unit (INU Stage Top Incubator, Tokai Hit, Shizuoka-ken, Japan). All culture dishes were kept in the chamber at 37°C for 10 min before images were acquired. This was done to allow to ensure that all dishes were imaged at the same time after labeling. Qdot 565 was excited using a 488 nm laser and acquired with an emission filter (600/50). Videos were acquired at a rate of 20 frames/s.

TIRF Microscopy

GFP-CLC was found to bleach rapidly using the spinning disk confocal, so for concurrent imaging of GFP-CLC and the MOR, total internal reflection fluorescence (TIRF) microscopy was performed on a Nikon Eclipse Ti fluorescence microscope equipped with a Perfect-Focus system, AOTF-controlled 488 and 647nm diode lasers, a 512x512 Andor iXon EMCCD DU-897 camera, and Plan Apo TIRF 100, NA 1.49 objective. Temperature was maintained at 37°C using Zeiss stage and objective heaters. Qdot 655 was used instead of Qdot 565 to avoid bleed-through into the 488 channel for imaging CLC-GFP. To avoid analyzing Qdots that occasionally were stuck to the culture dish glass, trajectories with MSDs characteristic of glass-stuck particles were removed before analysis. A sample of glass-stuck Qdots were imaged and found to have mostly MSDs below 0.0165 μm^2 (Fig. S3A). Therefore, all trajectories with an MSD less than 0.0165 μm^2 (measured up to a lag time of 2.5 s) were excluded from the data prior to analysis.

Image Processing and Analysis

Images were background-subtracted in ImageJ software. A Gaussian kernel filter was then applied to the images using a standard deviation of 0.8 pixels. After processing, Qdot-labeled MORs were detected and tracked using the u-track algorithm in MATLAB as previously described [38]. Detection of CLC-GFP puncta was also performed using the u-track algorithm. MOR trajectories less than 60 frames in length were excluded from further analysis.

Trajectories were analyzed in terms of the time-averaged mean square displacement (TA-MSD) using algorithms written in MATLAB. For an individual trajectory the TA-MSD is obtained by averaging over the time series,

$$\overline{\delta^2(t_{lag})} = \frac{1}{T - t_{lag}} \int_0^{T-t_{lag}} |\mathbf{r}(t + t_{lag}) - \mathbf{r}(t)|^2 dt, \quad (1)$$

where $\overline{\delta^2(t_{lag})}$ is the TA- MSD, $\mathbf{r}(t)$ is the two-dimensional position of the particle at time t, t_{lag} is the lag time (the time over which the displacement is computed), and T is the duration of the trajectory. For normal diffusion processes, the MSD scales linearly in lag time, namely in two dimensions $\overline{\delta^2(t_{lag})} = 4Dt_{lag}$, where D is the diffusion coefficient. However, measurements in live cells often exhibit anomalous diffusion, which manifests as a deviation from this simple law [20–22], and is characterized by a non-linear scaling of the MSD, $\overline{\delta^2(t_{lag})} = K_\alpha t_{lag}^\alpha$, where α is the anomalous exponent and K_α is the generalized diffusion coefficient which has units of cm^2/s^α. Processes with $0 < \alpha < 1$ are considered subdiffusive, and those with $\alpha > 1$ are considered superdiffusive. Detection uncertainty increases the MSD

by a constant value. Given a standard deviation σ of the detected position in both x and y direction due to uncertainty in the localization, the MSD is then

$$\overline{\delta^2(t_{lag})} = K_\alpha t_{lag}^\alpha + 4\sigma^2. \quad (2)$$

In order to obtain α and K_α from individual trajectories, we first obtained an average σ of 0.02 with the u-track algorithm and subtracted $4\sigma^2$ to obtain a static error-corrected MSD (see Fig. S3B for a histogram of localization uncertainties,σ). Then we perform a linear regression in log-log plot to find α and K_α.

To separate mobile tracks into free and confined portions, recurrence analysis was performed as described previously [30]. Briefly, a circle is constructed equal to the diameter of two consecutive points in a trajectory, and the number of subsequent visits by the particle into this circle was calculated. Portions of tracks with subsequent visits ≥ 11 were classified as confined portions of mobile trajectories, and those that did not reach this threshold were classified as free portions. This threshold was determined by identifying the minimum number of visits at which most immobile ($\alpha < 0.27$) trajectories were classified as confined.

To calculate the colocalization and distance of the MOR to CCPs, spatial coordinates of GFP-CLC puncta were determined using the detection output in u-track. The coordinates of GFP-CLC puncta were then compared to the coordinates of MOR tracks files at each frame. MOR coordinates that were located within 3 pixels of the closest GFP-CLC pit center (0.48 μm) were considered to be colocalized.

Statistical Analysis

Data sets were compared using an unpaired Kruskall-Wallis one way ANOVA with post hoc tests performed with Bonferroni correction, and p values of less than 0.05 were considered significant. Prism was used to perform statistical tests as well as to obtain descriptive statistics. Compiled data are shown as the mean ± SEM, or as histograms.

ACKNOWLEDGMENTS

The authors thank Dr. Michael Tamkun and his group for providing expertise and equipment necessary to carry out these studies. In particular, Emily Maverick and Dr. Laura Solé provided critical assistance in imaging and single-particle tracking. Additionally, we thank Dr. Sanaz Sadegh, Kanti Nepal, and Xinran Xu for providing technical assistance with MATLAB codes used for data analysis. Funding for these studies was provided by National Institutes of Health grants R01DA032562 (S.T.H.) and F31DA035586 (R.L.P.), as well as National Science Foundation grants DGE-1321845 (M.J.M) and 1401432 (D.K.).

[1] Williams, J. T., Christie, M. J. & Manzoni, O. Cellular and synaptic adaptations mediating opioid dependence. *Physiol Rev* **81**, 299-343, doi:10.1152/physrev.2001.81.1.299 (2001).

[2] Williams, J. T. et al. Regulation of mu-opioid receptors: desensitization, phosphorylation, internalization, and tolerance. *Pharmacol Rev* **65**, 223-254, doi:10.1124/pr.112.005942 (2013).

[3] Carayon, K. et al. Heterologous regulation of Mu-opioid (MOP) receptor mobility in the membrane of SH-SY5Y cells. *J Biol Chem* **289**, 28697-28706, doi:10.1074/jbc.M114.588558 (2014).

[4] Daumas, F. et al. Confined diffusion without fences of a g-protein-coupled receptor as revealed by single particle tracking. *Biophys J* **84**, 356-366, doi:10.1016/S0006-3495(03)74856-5 (2003).

[5] Halls, M. L. et al. Plasma membrane localization of the mu-opioid receptor controls spatiotemporal signaling. *Sci Signal* **9**, ra16, doi:10.1126/scisignal.aac9177 (2016).

[6] Melkes, B., Hejnova, L. & Novotny, J. Biased mu-opioid receptor agonists diversely regulate lateral mobility and functional coupling of the receptor to its cognate G proteins. *Naunyn Schmiedebergs Arch Pharmacol* **389**, 1289-1300, doi:10.1007/s00210-016-1293-8 (2016).

[7] Sauliere-Nzeh Ndong, A. et al. Agonist-selective dynamic compartmentalization of human Mu opioid receptor as revealed by resolutive FRAP analysis. *J Biol Chem* **285**, 14514-14520, doi:10.1074/jbc.M109.076695 (2010).

[8] Suzuki, K., Ritchie, K., Kajikawa, E., Fujiwara, T. & Kusumi, A. Rapid hop diffusion of a G-protein-coupled receptor in the plasma membrane as revealed by single-molecule techniques. *Biophys J* **88**, 3659-3680, doi:10.1529/biophysj.104.048538 (2005).

[9] Vukojevic, V. et al. Mu-opioid receptor activation in live cells. *FASEB J* **22**, 3537-3548, doi:10.1096/fj.08-108894 (2008).

[10] Haberstock-Debic, H. et al. Morphine acutely regulates opioid receptor trafficking selectively in dendrites of nucleus accumbens neurons. *J Neurosci* **23**, 4324-4332 (2003).

[11] Stoeber, M. et al. A Genetically Encoded Biosensor Reveals Location Bias of Opioid Drug Action. *Neuron* **98**, 963-976 e965, doi:10.1016/j.neuron.2018.04.021 (2018).

[12] Yu, Y. J., Dhavan, R., Chevalier, M. W., Yudowski, G. A. & von Zastrow, M. Rapid delivery of internalized signaling receptors to the somatodendritic surface by sequence-specific local insertion. *J Neurosci* **30**, 11703-11714, doi:10.1523/JNEUROSCI.6282-09.2010 (2010).

[13] Borgland, S. L., Connor, M., Osborne, P. B., Furness, J. B. & Christie, M. J. Opioid agonists have different efficacy profiles for G protein activation, rapid desensitization, and endocytosis of mu-opioid receptors. *J Biol*

Chem **278**, 18776-18784, doi:10.1074/jbc.M300525200 (2003).

[14] Celver, J., Xu, M., Jin, W., Lowe, J. & Chavkin, C. Distinct domains of the mu-opioid receptor control uncoupling and internalization. *Mol Pharmacol* **65**, 528-537, doi:10.1124/mol.65.3.528 (2004).

[15] Knapman, A. & Connor, M. Fluorescence-based, high-throughput assays for mu-opioid receptor activation using a membrane potential-sensitive dye. *Methods Mol Biol* **1230**, 177-185 (2015).

[16] Yousuf, A. et al. Role of Phosphorylation Sites in Desensitization of micro-Opioid Receptor. *Mol Pharmacol* **88**, 825-835, doi:10.1124/mol.115.098244 (2015).

[17] Thompson, G. L. et al. Systematic analysis of factors influencing observations of biased agonism at the mu-opioid receptor. *Biochem Pharmacol* **113**, 70-87, doi:10.1016/j.bcp.2016.05.014 (2016).

[18] Dang, V. C. & Christie, M. J. Mechanisms of rapid opioid receptor desensitization, resensitization and tolerance in brain neurons. *Br J Pharmacol* **165**, 1704-1716, doi:10.1111/j.1476-5381.2011.01482.x (2012).

[19] Knapman, A. et al. A continuous, fluorescence-based assay of mu-opioid receptor activation in AtT-20 cells. *J Biomol Screen* **18**, 269-276, doi:10.1177/1087057112461376 (2013).

[20] Höfling, F. & Franosch, T. Anomalous transport in the crowded world of biological cells. *Rep Prog Phys* **76**, 046602, doi:10.1088/0034-4885/76/4/046602 (2013).

[21] Krapf, D. Mechanisms underlying anomalous diffusion in the plasma membrane. *Curr Top Membr* **75**, 167-207, doi:10.1016/bs.ctm.2015.03.002 (2015).

[22] Metzler, R., Jeon, J. H., Cherstvy, A. G. & Barkai, E. Anomalous diffusion models and their properties: non-stationarity, non-ergodicity, and ageing at the centenary of single particle tracking. *Phys Chem Chem Phys* **16**, 24128-24164, doi:10.1039/c4cp03465a (2014).

[23] Akin, E. J. et al. Single-molecule imaging of Nav1.6 on the surface of hippocampal neurons reveals somatic nanoclusters. *Biophys J* **111**, 1235-1247, doi:10.1016/j.bpj.2016.08.016 (2016).

[24] Weron, A. et al. Ergodicity breaking on the neuronal surface emerges from random switching between diffusive states. *Sci Rep* **7**, 5404, doi:10.1038/s41598-017-05911-y (2017).

[25] Michalet, X. et al. Quantum dots for live cells, in vivo imaging, and diagnostics. *Science* **307**, 538-544, doi:10.1126/science.1104274 (2005).

[26] Pinaud, F., Clarke, S., Sittner, A. & Dahan, M. Probing cellular events, one quantum dot at a time. *Nat Methods* **7**, 275-285, doi:10.1038/nmeth.1444 (2010).

[27] Weigel, A. V., Simon, B., Tamkun, M. M. & Krapf, D. Ergodic and nonergodic processes coexist in the plasma membrane as observed by single-molecule tracking. *Proc Natl Acad Sci U S A* **108**, 6438-6443, doi:10.1073/pnas.1016325108 (2011).

[28] Abraham, L. et al. Limitations of Qdot labelling compared to directly-conjugated probes for single particle tracking of B cell receptor mobility. *Sci Rep* **7**, 11379, doi:10.1038/s41598-017-11563-9 (2017).

[29] Arttamangkul, S., Alvarez-Maubecin, V., Thomas, G., Williams, J. T. & Grandy, D. K. Binding and internalization of fluorescent opioid peptide conjugates in living cells. *Mol Pharmacol* **58**, 1570-1580 (2000).

[30] Sikora, G. et al. Elucidating distinct ion channel populations on the surface of hippocampal neurons via single-particle tracking recurrence analysis. *Phys Rev E* **96**, 062404, doi:10.1103/PhysRevE.96.062404 (2017).

[31] Gaidarov, I., Santini, F., Warren, R. A. & Keen, J. H. Spatial control of coated-pit dynamics in living cells. *Nat Cell Biol* **1**, 1-7, doi:10.1038/8971 (1999).

[32] Kirchhausen, T. Imaging endocytic clathrin structures in living cells. *Trends Cell Biol* **19**, 596-605, doi:10.1016/j.tcb.2009.09.002 (2009).

[33] Weigel, A. V., Tamkun, M. M. & Krapf, D. Quantifying the dynamic interactions between a clathrin-coated pit and cargo molecules. *Proc Natl Acad Sci U S A* **110**, E4591-4600, doi:10.1073/pnas.1315202110 (2013).

[34] Zhao, H., Loh, H. H. & Law, P. Y. Adenylyl cyclase superactivation induced by long-term treatment with opioid agonist is dependent on receptor localized within lipid rafts and is independent of receptor internalization. *Mol Pharmacol* **69**, 1421-1432, doi:10.1124/mol.105.020024 (2006).

[35] Zheng, H., Chu, J., Qiu, Y., Loh, H. H. & Law, P. Y. Agonist-selective signaling is determined by the receptor location within the membrane domains. *Proc Natl Acad Sci U S A* **105**, 9421-9426, doi:10.1073/pnas.0802253105 (2008).

[36] Sungkaworn, T. et al. Single-molecule imaging reveals receptor-G protein interactions at cell surface hot spots. *Nature* **550**, 543-547, doi:10.1038/nature24264 (2017).

[37] Birdsong, W. T., Arttamangkul, S., Bunzow, J. R. & Williams, J. T. Agonist Binding and Desensitization of the mu-Opioid Receptor Is Modulated by Phosphorylation of the C-Terminal Tail Domain. *Mol Pharmacol* **88**, 816-824, doi:10.1124/mol.114.097527 (2015).

[38] Jaqaman, K. et al. Robust single-particle tracking in live-cell time-lapse sequences. *Nat Methods* **5**, 695-702, doi:10.1038/nmeth.1237 (2008).